Performance Evaluation of an Advanced XRF Elemental Mapping System Featuring a Novel Ring-Shaped Monolithic Array of Silicon Drift Detectors

R. Alberti, S. Buzzetti, *Member, IEEE*, C. Fiorini, *Member, IEEE*, C. Guazzoni, *Member, IEEE*, T. Klatka, P. Lechner, A. Longoni, L. Strüder,

***Abstract*— This paper introduces an ultra-fast x-ray fluorescence (XRF) spectrometer based on a novel ring-shaped Semiconductor Drift Detector (SDD) and on a novel readout and processing electronics and discusses its performance. The new detector is based on 4 independent "droplet" type SDDs monolithically integrated on the same chip. The detector shape optimizes the collection angle of the fluorescence radiation. The x-ray excitation beam is focused on the sample by means of a polycapillary lens through the hole cut in the center of the detector. The "droplet" type SDD is characterized by a better energy resolution and a better peak-to-valley ratio with respect to the ones of "conventional" SDDs. The energy resolution is of the order of 140 eV FWHM on the Mn Kα line with 1 μs shaping time at -15°C and the peak-to-valley ratio is of the order of 6000. In order to fully exploit the detection rate performance of this detector we have developed a novel read-out electronic unit with selectable shaping time and on-board histogramming capability.**

***Index Terms*—x-ray fluorescence, Silicon Drift Detector, Elemental Mapping, ultra-fast X-ray spectrometer.**

I. Introduction

SEVERAL analytical techniques are based on the detection of the x-rays emitted by the atoms of a specimen excited by a primary beam (electrons, protons, ionized particles or x-rays). The X-Ray Fluorescence (XRF) [1] is an inherently non-destructive technique, based on the specimen excitation by means of a primary x-ray beam. Particular strengths of this analytical method include easy sample preparation, analysis of electrically non-conducting materials (notably oxides, glasses, ceramics and biological samples), and possibility of keeping the sample in air and of operating in-situ.

Recent technological developments and new topology designs made Semiconductor Drift Detectors ideal devices for high-resolution x-ray spectroscopy. The Semiconductor Drift Detector, invented by E. Gatti and P. Rehak in 1983, is characterized by low output capacitance (of the order of 100 fF), independent of the active area. The SDD [2], due to its very small output capacitance, can reach energy resolutions approaching the ones of liquid-nitrogen cooled detectors, with the advantage of a much shorter shaping time (shorter than 1 μs) [3]. The availability of high-resolution, high-count-rate SDDs opened the way to the development of high-resolution compact spectrometers suitable for non-destructive analyses of materials [4]-[8]. All these developments are based on a single element detector. In [9]-[11] we have presented the design and performance of an innovative x-ray fluorescence spectrometer designed to achieve high energy and position resolution in elemental mapping applications. That spectrometer was based on a monolithic array of 12 conventional Semiconductor Drift Detectors (SDD) cooled by a Peltier element. The subdivision of the total active area in several independent detectors allows the increase of the maximum counting rate of the system with respect to a single detector of the same total active area since in general the maximum photon flux is limited by pulse pile-up both in the detector itself and in the readout electronics. The possibility of having different readout channels operating in parallel allows a higher degree of freedom in the choice of the optimum shaping time with respect to a single readout channel for a given count rate. The 12 SDD cells are arranged in a closed ring around a hole laser-cut in the center of the chip. The particular structure of the detector array allows the transport of the x-ray excitation beam to the sample through the hole in the center of the array, thus optimizing the solid angle for the collection of the x-ray fluorescence. The x-ray excitation beam (generated by a micro-focus tube) is focused through this hole on the sample by means of a capillary optics system

Manuscript received October 17, 2006. This work was supported by INFN - Sezione di Milano under the FELIX experiment and partly by Politecnico di Milano - Progetto Giovani Ricercatori.

R. Alberti, S. Buzzetti, C. Fiorini, C. Guazzoni, T. Klatka and A. Longoni, are with Politecnico di Milano, Dipartimento di Elettronica e Informazione, Piazza Leonardo da Vinci, 32, 20133 Milano, Italy and with INFN, Sezione di Milano, Italy. (telephone: +39 02 2399-6104, e-mail: antonio.longoni@polimi.it). A. Longoni is also wth IFN-CNR, Sezione di Milano.

L. Strüder is with the Max Planck Institut für Extraterrestriche Physik, Giessenbachstrasse, 85741 Garching, Germany and with MPI-Halbleiterlabor, Otto-Hahn-Ring 6, München D-81739, Germany.

P.Lechner is with PNSensor GmbH, Römerstrasse 28, 80803 München, Germany and with MPI-Halbleiterlabor, Otto-Hahn-Ring 6, München D-81739, Germany.

[12]. The spot diameter of the x-ray beam focused on the sample has a gaussian shape with about 80 μm FWHM. Since the emission of X-ray fluorescence is nearly isotropic the spot diameter gives the position resolution of the system. In order to be able to detect details of small dimensions the system need a good modulation transfer function (MTF) that is determined by the spot size on the sample [11]. All these features guarantee high performance in terms of energy resolution, spatial resolution and maximum count rate.

Reference [13] reports of the application of the same annular 12 element SDD in μPIXE applications at Sandia National Laboratories.

Recently, we have significantly improved the performance of our spectrometer, in terms of energy resolution and detection rate, with the design and the introduction of a novel ring-shaped SDD and of novel fast read-out electronics. In this paper we report the performance evaluation of this novel XRF spectrometer for elemental mapping. Section II describes the main design features and performance of the novel spectrometer in terms of both the detector and the data-acquisition system (DAQ). Section III presents a selection of the measurements carried out to qualify the spectrometer performance in different fields of application, from the analysis of works of art to that of geological samples. Section IV ends with the conclusions.

II. Advanced XRF elemental mapping system

Fig. 1 shows the conceptual design of the measurement head of the proposed spectrometer for elemental mapping. A micro-focus x-ray generator, equipped with a W anode and coupled to a polycapillary x-ray lens focuses the primary beam on the sample through the hole laser-cut in the center of the detector chip. The polycapillary lens concentrates a high photon flux on a small spot on the sample, with a diameter of a few tens of micrometers, which guarantees high spatial resolution and the detector-sample geometry allows the collection of a large fraction of the emitted fluorescence. Moreover, the distance between the sample and the detector can be reduced with a corresponding reduction of air absorption on the fluorescence radiation coming from light elements. These features, together with the high detection rate of the SDDs, shorten the scanning time in elemental mapping since operation at several tens of kcps with no energy resolution degradation is possible and up to several hundred of kcps the worsening of the energy resolution is negligible [3]. A charge preamplifier configuration can be applied to this spectrometer and allows peaks stability up to very high count rates (several hundred of kcps) [14]. If the charge preamplifier is equipped with pulse reset no energy resolution degradation is observable up to several hundred of kcps. Scanning time in elemental mapping applications as short as 0.5 s per point are possible as shown in [11].

A sealed case (not shown in the Figure) filled with dry nitrogen and equipped with a beryllium window – towards the x-ray generator – and a Mylar window – towards the sample under analysis – houses the detector chip cooled by Peltier elements. An X-Y remotely-controlled stage is responsible of sample scanning. The readout and processing of the signals coming from the detector is accomplished with custom-designed electronics. Dedicated software, running on a host PC, takes care of the acquisition of the spectra, of the X-Y scanning of the sample and of data storing and processing.

A. Four-element Silicon Drift Detector Droplet Design and Performance

A ring-shaped detector constituted by a monolithic array [3] of four Silicon Drift Detectors of the novel “droplet” type [4] is the core of the spectrometer. Fig. 2a shows the topology of the detector. The total active area of the 4-element detector is about 60 mm^2 (15 mm^2 per detector element) and it reduces to about 50 mm^2 by screening the anode and transistor regions. The four detectors surround the central hole (4 mm diameter) that is separated from the active area by a properly designed guard region. The hole laser-cut in the center of the ring lets the excitation beam reach the sample. The detector thickness is 450 μm. The subdivision of the area in four independent detectors increases the maximum count rate of the system with respect to a single detector with the same area and reduces the number of output channels with respect to the previous 12-element configuration. The four SDDs can be biased independently in order to optimize their individual performance. The collecting anode of each SDD is moved away from the center of the active region towards the detector periphery and is located at the outside margin of the structure as shown in Fig. 2b. This new anode location allows the reduction of the anode dimensions. In fact, thanks to the asymmetry of the arrival path of the signal charge, the front end JFET can be integrated outside the anode. Consequently, the anode capacitance of the “droplet” type SDDs is lower than the one of the conventional type. The total capacitance at the transistor gate (anode, JFET gate and stray capacitances) is of the order of 120 fF, to be compared with the 230 fF output capacitance of a conventional SDD [15]. The energy resolution is consequently improved. Moreover, this geometry allows an easy screening of the anode and transistor regions by means of a collimator, with a consequent improvement of the peak-to-valley ratio in the collected spectrum.

Reference [10] and [11] report the results of the basic characterization of the novel four-element detector. Here we summarize the relevant results of the characterization of the detector installed and operative in the XRF spectrometer. The detector is cooled at about -15°C by the Peltier system included in the measurement head of the spectrometer. The insets of Fig. 2 show the typical spectra measured at each channel when a ^{55}Fe radioactive source illuminates the detector active area with no collimation at about 5 kcps per channel. The measured average resolution at 1 μs pseudo-Gaussian shaping time is about 140 eV FWHM at the Mn Kα line, with a good uniformity among the four channels. The peak-to-background ratio (defined as the ratio between the peak value of the Mn Kα line and the average value of the

shoulder evaluated between 800 eV and 1200 eV) is of the order of 6000 with a beam collimation of 500μm.

We scanned the whole area of the silicon chip with a collimated broadband x-ray beam (about 250 μm diameter) with 250 μm step in order to test the uniformity of the detection efficiency of the detector. To perform this analysis we mounted the measurement head with the detector bottom-side up and used the Tungsten anode x-ray generator and the capillary optics of the spectrometer to focus the x-ray beam on the silicon chip. Fig. 3 shows the map of the total collected counts. The response shows good uniformity for the four SDDs and a very limited dead region in the transistor region that can be screened.

In order to evaluate the performance of the spectrometer in the detection of trace elements a first set of measurements has been carried out with different dilutions of a solution of iodine in isopropyl alcohol (C_3H_8O). Fig. 4 shows the integral of the counts in the iodine Lα line as a function of the iodine concentration (0.3 ml of solution poured in a 10 mm diameter and 5 mm deep hole in a Lucite phantom). The measurement of each point of the curve lasted 500 s. The figure shows a good linearity of the detected points. At a concentration of 20 μg/ml (about 20ppm) at the Lα iodine line (3.94 keV) the ratio between the counts under the peak and the background standard deviation is greater than 7. We did not probe lower concentrations due to technical difficulties in the titration of solutions at concentrations below 20 ppm.

B. Data Acquisition System architecture and performance

In order to fully exploit the detector performance, a novel, complete four-channel acquisition system has been designed and realized [16]. Fig. 5 shows its basic structure. It consists of four main sections: analog, digital, motion control and user interface.

The analog section includes four 5th order pseudo-Gaussian shaping amplifiers with user selectable shaping time (150 ns for high rate measurements and 450 ns for high resolution measurements) and four fast amplifiers (30 ns shaping time constant) to provide the trigger signals for the pile-up rejection unit (PUR).

The digital section is based on a field-programmable gate array (FPGA), which controls the data acquisition process and stores the four spectra in the on-chip random access memory (RAM). The amplitude of peak pulse is caught by a peak-stretcher and then multiplexed into one signal line, which is sampled by a single 10 MSPS 14-bit analog-to-digital converter (ADC).

The motion control section takes care of the automatic scan of the sample area under analysis.

The user interface serves for data reading from the FPGA through the EPP bus and for the visualization and analysis of the acquired data. Moreover it provides statistical information for each spectrum such as counts/second, total counts, dead time, peaks fitting parameters and on-line area maps visualization. A USB communication port is under development.

Several tests, such as shaper transfer function, noise performance, and PUR functionality have been carried out and are reported in [16]. In this paper we present the rate performance characterization. Measurements of the output throughput were performed using a frequency-adjustable random pulse generator connected to the shaping amplifier as well as using the four-channel SDD irradiated with a ^{55}Fe source at different detector-source distances. Results obtained in the first case give a maximum throughput of 200 kcps per channel at 450 ns shaping time and of 0.9 Mcps at 150 ns shaping time (with PUR disabled). Fig. 6 shows the measured throughput at 150 ns and 450 ns shaping time with the detector irradiated with a ^{55}Fe radioactive source (PUR disabled) for one channel. The present activity of the source (about 5 mCi) limits the maximum photon flux that can be obtained on the active area of a single detector element to about 250 kpcs. The figure also shows the best fit of the experimental points assuming a paralyzable dead-time model [17]. Similar performance is obtained on all the channels.

III. Elemental Mapping Examples

The proposed XRF spectrometer is well suited for non-destructive elemental mapping analyses in different fields of application. Several results, obtained with the old 12-element detector and with a preliminary version of the spectrometer, are reported in [9]-[11]. Here, as an example of the analyses obtained with the new 4-element device installed in the new version of the spectrometer, we present the study of the elemental distribution in fossils. The high voltage of the x-ray generator was set to 30kV and the current to 300 μA. Fig. 7a shows a schematic drawing of one of the analyzed fossils, a Trilobite (order Agnostida). The elemental map is obtained in real time. The scanned area is about 5 mm × 8 mm with 300 μm × 300 μm pitch. With an acquisition time of 2 s per point the total measurement time is about 900s. The average count rate was in this case more than 10kcps per channel. Fig. 7b shows the map of the calcium distribution while Fig. 7c shows the iron distribution. As can be noticed from the elemental mapping in the fossil region there is an abundance of calcium while the substrate is mainly composed of iron whose fluorescence is absorbed by the calcium layer in the fossil area. Fig. 7d shows long-acquisition time (2800 s) spot spectra (four adjacent points have been measured and the corresponding spectra summed) in the Trilobita area (point 1 of map shown in Fig. 7b) and in the external region (point 2 of map shown in Fig. 7b).

In cooperation with the Civic Archaeological Museum of Milano a campaign of analyses of Lombard finds of the 7th century (found in graves in North of Italy) was performed. An overview of this kind of artifacts is given in [18]. Several artifacts were analyzed providing the map of their elemental composition. The central photograph of Fig. 8 shows a detail of one of the analyzed inlaid works (agemina). The result of the elemental mapping analysis is shown in Fig. 8, too. On the substrate thin strips of silver and brass have been inserted by the craftsman in narrow engravings whose transverse

dimensions are of the order of some hundreds micrometers. The scanned area is 4mm x 4mm with 250 μm pitch. The acquisition time is 2 s for each measurement point. The composition of the different alloys has been determined, too. Table I shows the results for the agemina shown in Fig. 8. The substrate is mainly composed of iron. The analyses of other inlaid works found in the same grave show the use also of strips of gold by the Lombard craftsmen.

IV. Conclusions

In this paper we reported the performance evaluation of a fast XRF spectrometer for elemental mapping based on a novel monolithic array of four SDDs, on a polycapillary lens and on novel fast read-out electronics. The spectrometer can perform non-destructive analyses of samples and objects in air. The scanning rate can be ultra-fast owing to the peculiar geometry of the detector, to the high count-rate capability of the SDDs and to the dedicated read-out electronics. The quantum efficiency at low energies is improved thanks to the short distance between the sample and the detector.

The spectrometer has been evaluated in different fields of application, from the analysis of works of art to that of geological samples and a selection of the measurements carried out to qualify the spectrometer performance has been reported in the paper.

Acknowledgment

We would like to thank the staff of the Halbleiterlabor of the Max Plank Institut and of PNSensor for detector design and production. IfG GmbH has produced the micro focus generator with the polycapillary lens. We acknowledge F. Bonomelli and F. Moia for their help in the experimental measurements, G. Valenti for the collaboration in the DAQ development, S. Masci for the careful bonding of the detector prototype, L. Pallaro for the mechanical setup and M. Ortenzi for the preparation of the chemical solutions used for the detection limit evaluation.

References

[1] A. T. Ellis, "Energy-Dispersive X-Ray Fluorescence Analysis Using X-ray Tube Excitation", in *Handbook of X-Ray Spectrometry*, 2nd Edition, R. Van Grieken and A. Markowicz, Eds. Marcel Dekker, Inc., Series: Practical Spectroscopy Vol. 29, 2001 ISBN: 0824706005.

[2] E.Gatti and P.Rehak, "Semiconductor Drift Chamber - An application of a novel Charge Transport Scheme," *Nucl. Instr. Meth.*, vol. A 225, pp. 608-614, 1984.

[3] P. Lechner, S. Eckbauer, R. Hartmann, S. Krisch, D. Hauff, R. Richter, H. Soltau, L. Strüder, C. Fiorini, E. Gatti, A. Longoni, M. Sampietro, “Silicon drift detectors for high resolution room temperature x-ray spectroscopy,” *Nucl. Instr. Meth.*, vol. A 377, pp. 346-351, 1996.

[4] C. Fiorini, A. Longoni, “In-situ, non-destructive identification of chemical elements by means of portable EDXRF spectrometer”, *IEEE Trans. on Nucl. Sci*., Vol. 46, n° 6, p. 2011-2016, 1999.

[5] H. Bronk, S. Röhrs, A. Bjeoumikhov, N. Langhoff, J. Schmalz, R. Wedell, H.-E. Gorny, A. Herold, U. Waldschläger, "ArtTAX - a new mobile spectrometer for energy-dispersive micro X-ray fluorescence spectrometry on art and archaeological objects", Fresenius' Journal of Analytical Chemistry, Vol. 371, pp. 307-316, 2001.

[6] D. Wegrzynek, A. Markowicz, S. Bamford, E. Chinea-Cano, M. Bogovac, “Micro-beam X-ray fluorescence and absorption imaging techniques at the IAEA Laboratories”, *Nucl. Instr. Meth.*, vol B 231 2005, pp. 176–182.

[7] Dale E. Newbury, “The New X-ray Mapping: X-ray Spectrum Imaging above 100 kHz Output Count Rate with the Silicon Drift Detector”, *Microsc. Microanal.* vol. 12, 2006, pp. 26–35.

[8] V. Desnica, M. Schreiner, “A LabVIEW-controlled portable x-ray fluorescence spectrometer for the analysis of art objects”, *X-ray Spectrometry*, Vol. 35, Sept.-Oct. 2006, pp. 280-286.

[9] A.Longoni, C.Fiorini, C.Guazzoni, A.Gianoncelli, L.Strüder, H.Soltau, P.Lechner, A.Bjeoumikhov, J.Schmalz, N.Langhoff, R.Wedell, "A new XRF spectrometer based on a ring-shaped multi-element silicon drift detector and on x-ray capillary optics", *IEEE Trans. Nucl. Sci*., Vol. 49, no.3, June 2002, pp. 1001-1005.

[10] A.Longoni, C. Fiorini, C. Guazzoni, S. Buzzetti, M. Bellini, L. Strüder, P. Lechner, A. Bjeoumikov, J. Kemmer, "A novel high resolution XRF spectrometer for elemental mapping based on a monolithic array of Silicon Drift Detectors and on a polycapillary x-ray lens", *X-ray Spectrometry*, Vol. 34, 2005, pp. 439-445; DOI:10.1002/xrs.858.

[11] A. Longoni, C. Fiorini, C. Guazzoni, S. Buzzetti, M. Bellini, ,L. Strüder, P. Lechner, A. Bjeoumikov and J. Kemmer, "XRF Spectrometers based on Monolithic Arrays of Silicon Drift Detectors: Elemental Mapping Analyses and Advanced Detector Structures", *IEEE Trans. Nucl. Sci*., Vol. 53 (2) April 2006, pp.:641 – 647.

[12] M. A. Kumachov, “Channeling of photons and new x-ray optics,” *Nucl. Instr. Meth.*, vol. B48, pp. 283-286, 1990.

[13] B. L. Doyle, D. S. Walsh, P. G. Kotula, P. Rossi, T. Schülein, M. Rohde, "An annular Si drift detector μPIXE system using AXSIA analysis", *X-Ray Spectrom.*, Vol. 34, pp. 279–284, 2005.

[14] R. Alberti, C. Fiorini, A. Longoni, H. Soltau "High-rate X-ray spectroscopy using a Silicon Drift Detector and a charge preamplifier" *Nucl. Instr. and Meth*,.A 568, 106-111, 2006

[15] P. Lechner, A. Pahlke, H. Soltau, “Novel high-resolution silicon drift detectors”, *X-ray Spectrometry*, Vol. 33, July/August 2004, pp. 256-261.

[16] S. Buzzetti, M. Capou, C. Guazzoni, A. Longoni, R. Mariani, S. Moser, " High-speed FPGA-based pulse-height analyzer for high resolution x-ray spectroscopy", *IEEE Trans. Nucl. Sci*., Vol. 52, no.4, August 2005, pp. 854-860.

[17] G. F. Knoll, Radiation Detection and Measurement, 3rd ed. NewYork: Wiley, 2000, pp.119–122.

[18] "La necropoli longobarda di Trezzo sull’Adda", edited by E. Roffia in the Series Ricerche di archeologia altomedievale e medievale, Vol. 12-13, All'insegna del Giglio, Firenze, 1986.

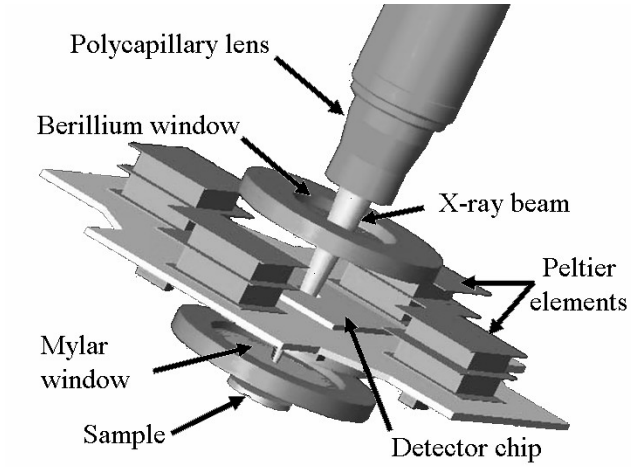

Fig. 1. Conceptual design of the measurement head of the proposed XRF spectrometer.

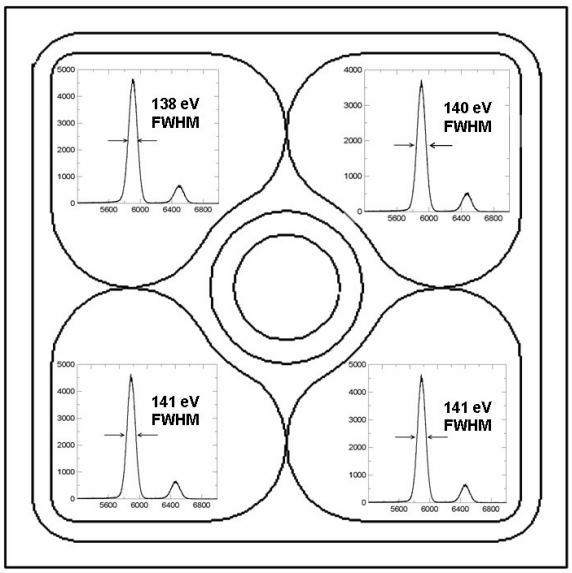

(a)

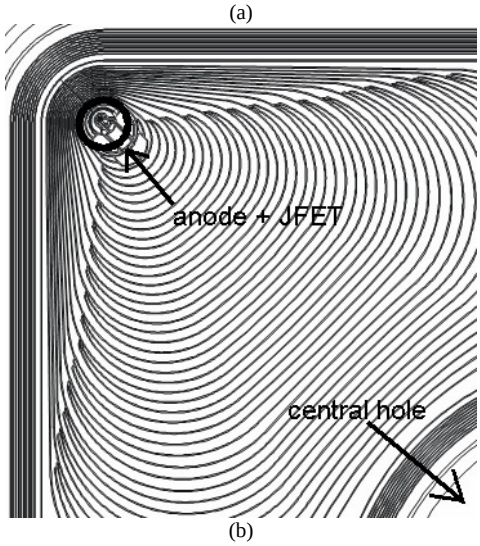

(b)

Fig. 2. a) Schematic layout of the new optimized version of the 4-channel SDD Droplet ring-detector. The insets show the typical spectrum at each channel when a ^{55}Fe source illuminates the detector. For measurement details see text. (b) Detailed view of the anode side of one of the four SDDs with the indication of the anode and on-chip JFET location.

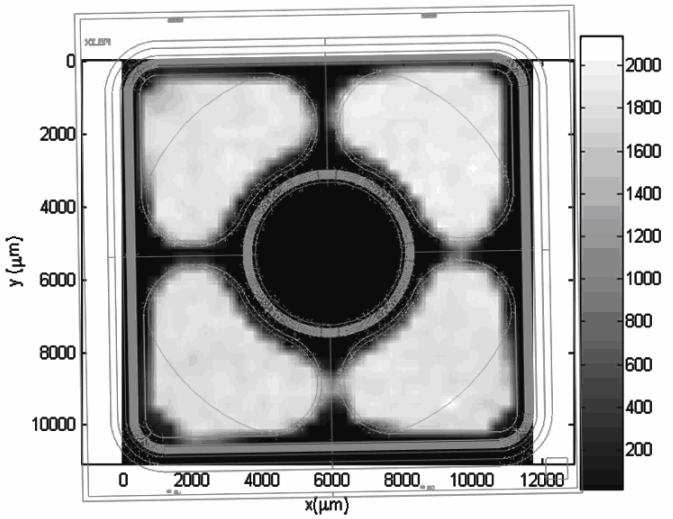

Fig. 3. Gray-scale map of the collected counts, showing the relative detection efficiency as a function of the position of interaction of the radiation. The layout of the detector (light grey lines) is superposed.

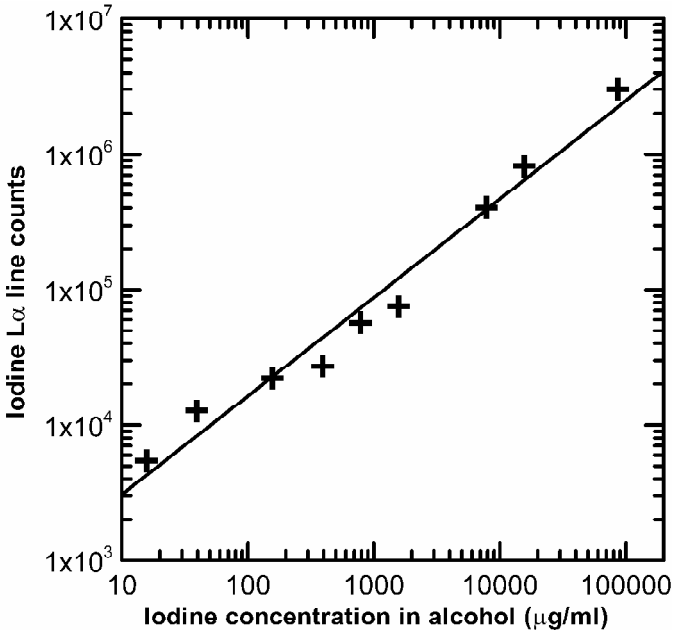

Fig. 4 Iodine Lα line intensity (integral of the counts) as a function of the iodine concentration in isopropyl alcohol.

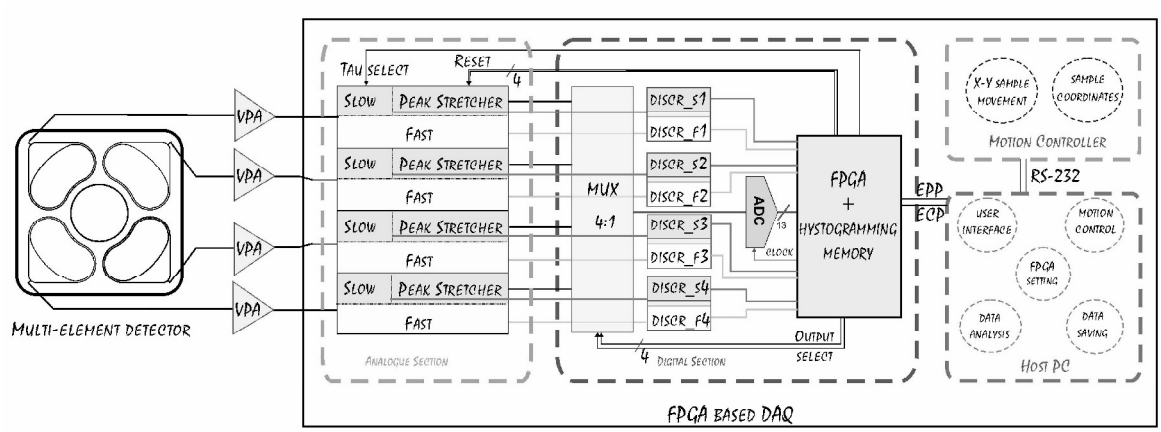

Fig. 5. Basic structure of the Data Acquisition System coupled to the 4-channel SDD Droplet ring-detector Four independent voltage preamplifiers (VPA) are used at the detector output. [9].

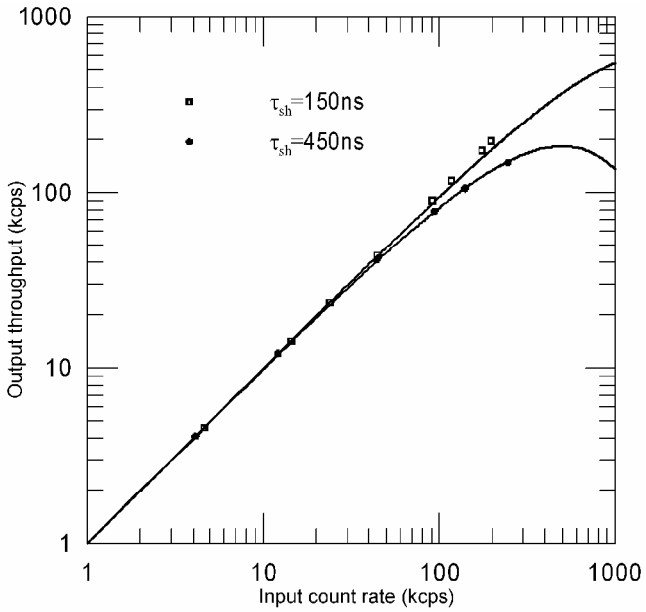

Fig. 6. Measured throughput for 150 ns and 450 ns shaping time with the detector irradiated with a ^{55}Fe radioactive source. The PUR was not active during the measurement. The continuous lines is the best fit of the data according to the paralyzable dead-time model [9].

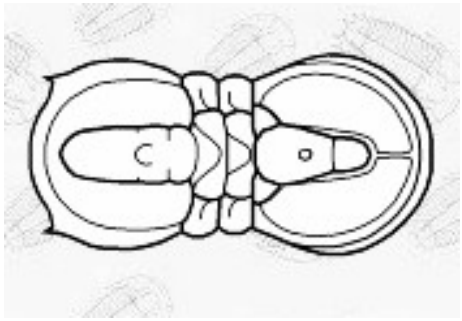

(a)

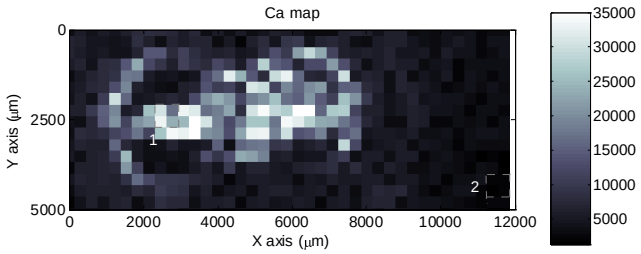

(b)

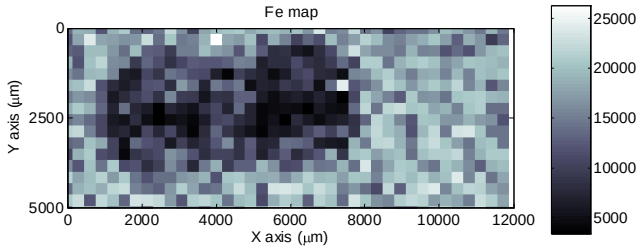

(c)

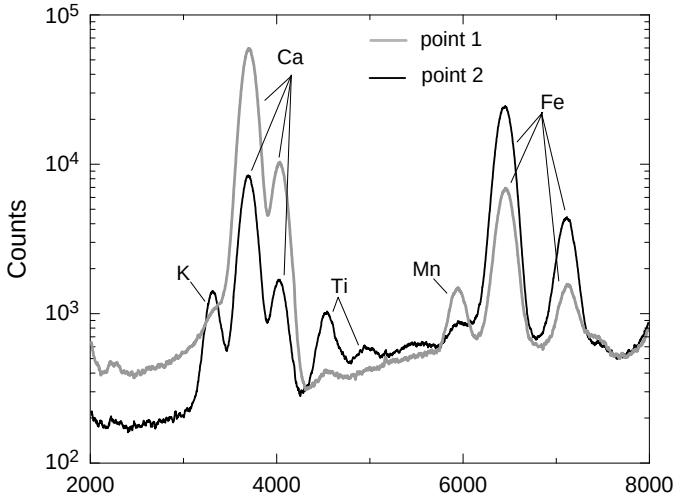

(d)

Fig. 7. a) Schematic draw of the analyzed fossil (Trilobite – order Agnostida). b) Map of the calcium distribution (integral of the counts at the Ca Kα line) of the analysed fossil. c) Map of the iron distribution (integral of the counts at the Fe Kα line) of the analysed fossil. d) Long-acquisition-time spot spectra measured in points 1 and 2 of Fig. 7b. See text for measurement details. The characteristic fluorescence lines of calcium and iron are clearly visible.

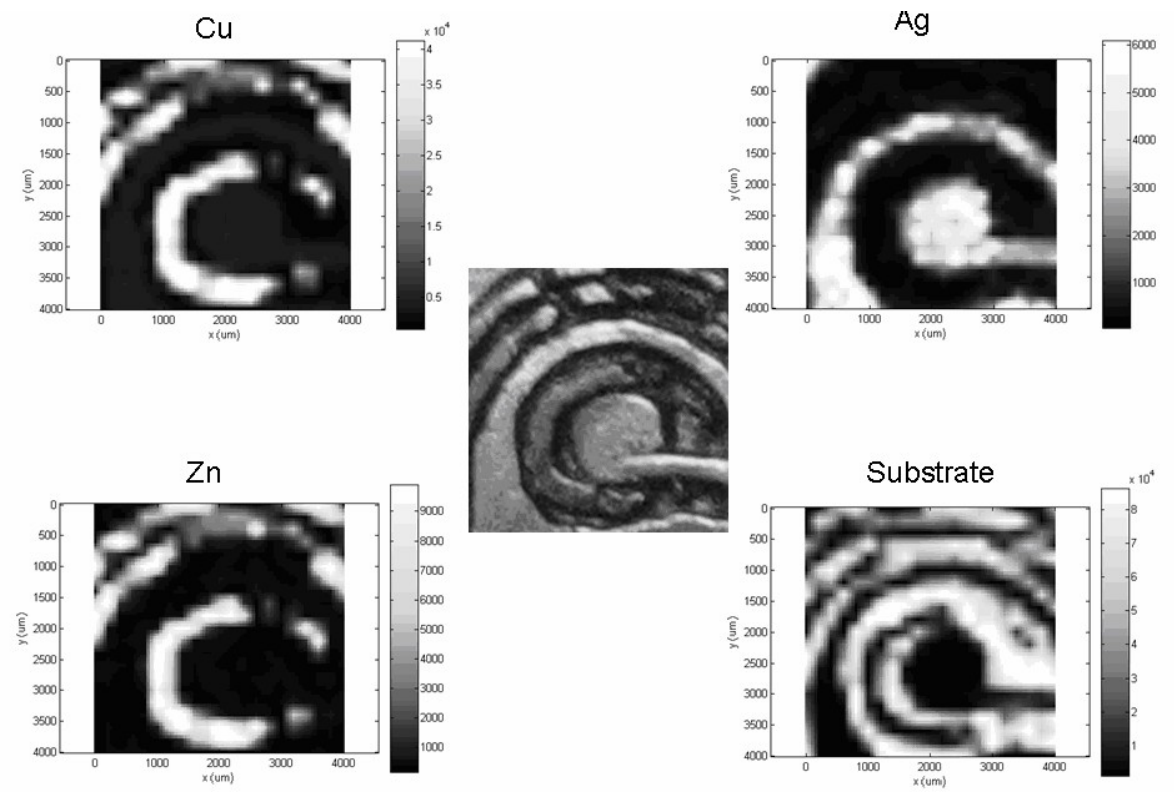

Fig. 8. Elemental mapping of a detail of a Lombard artifact. The photograph of the detail is shown in the center of the figure.

TABLE I
ELEMENT COMPOSITION OF THE AGEMINA SHOWN IN FIGURE 8

	SUBSTRATE	SILVER LAYER	BRASS LAYER
Fe	97.6%	1.4%	0.8%
Cu	2.2%	4.3%	78.8%
Zn	0%	0%	19.5%
Ag	0.2%	94.3%	0.9%